Journal of Materials Chemistry C

Accepted Manuscript

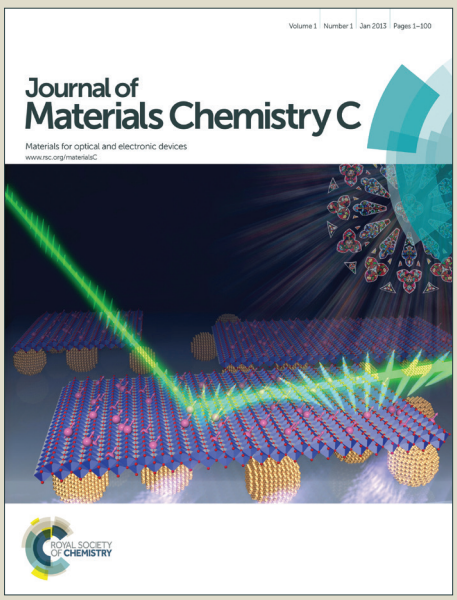

ROYAL SOCIETY OF CHEMISTRY

www.rsc.org/materialsC

Tuning into blue and red: europium single-doped nano-glass-ceramics for potential application in photosynthesis

Daqin Chen[a,b*], Zhongyi Wan[a], Yan Zhou[a], Weidong Xiang[c,*], Jiasong Zhong[a], Mingye Ding[a], Hua Yu[a], Zhenguo Ji[a,*]

[a] College of Materials & Environmental Engineering, Hangzhou Dianzi University, Hangzhou, 310018, P. R. China

[b] State Key Laboratory of Structural Chemistry, Fujian Institute of Research on the Structure of Matter, Chinese Academy of Sciences, Fuzhou, Fujian 350002, PR China

[c] College of Chemistry and Materials Engineering, Wenzhou University, Wenzhou, 325035, P. R. China

Abstract: A series of SiO_2-Al_2O_3-NaF-YF_3 oxyfluoride glasses and β-YF_3 nanocrystals embedded glass ceramics single-doped with europium ions were prepared by high-temperature melt-quenching to explore blue/red luminescent materials for potential application in photosynthesis of green plants. Both Eu^{2+} activators and Eu^{3+} ones were demonstrated to coexist in this special designed glass fabricated under ambient atmosphere, which can be well explained based on optical basicity model of glass and evidenced by emission, excitation and time-resolved spectra. Furthermore, crystallization strategy has been adopted to convert the precursor glasses into nano-glass-ceramics. As a result, Eu^{3+} ions partitioned into the precipitated orthorhombic YF_3 nanophase, while Eu^{2+} ones remained in the glass matrix. Such spatial isolation of the different active ions in glass ceramics can effectively suppress adverse energy transfer between Eu^{2+} and Eu^{3+}, leading to both intense Eu^{2+} blue and Eu^{3+} red emissions under ultraviolet light excitation.

Corresponding authors:
E-Mail: dqchen@hdu.edu.cn (D. Q. Chen);
xiangweidong001@126.com (W. D. Xiang);
jizg@hdu.edu.cn (Z. G. Ji)

Introduction

Photosynthesis is a process used by plants and other organisms to convert light energy, normally from the Sun, into chemical energy that can be later released to fuel the organisms' activities. The reaction, taking place between carbon dioxide and water to produce glucose and a waste product, oxygen, relies on the aid of chlorophyll [1-2]. In photosynthesis, electrons are transferred from water to carbon dioxide in a reduction process. Chlorophyll assists in this process by trapping solar energy. When chlorophyll absorbs energy from sunlight, an electron in the chlorophyll molecule is excited from a lower energy state to a higher one. The excited electron is more easily transferred to another molecule. A chain of electron-transfers move forwards, ending when the electron is captured by a carbon dioxide molecule.

Generally, the green plants (chlorophylls) absorb more reddish orange (600-700 nm) and bluish violet (380-480 nm) lights than other wavelengths in the course of the photosynthesis [3-4]. In the solar spectrum, the energy percentages of the ultraviolet, visible, and infrared light are 7%, 50%, and 43%, respectively [5]. The lights absorbed by green plants for photosynthesis are only a very small part in the whole solar spectrum. It will be an interesting work to improve the utilization of solar. A feasible way is to turn a photon, which cannot be efficiently absorbed by green plants, into another photon, which can be efficiently absorbed by green plants for photosynthesis.

In fact, spectrum modification is a well-investigated topic in physics and

chemistry, and has been applied, for example, to infrared quantum counters [6], efficient lamp phosphors [7] and solar cells [5, 8]. Lanthanide and transition metal ions have abundant excited states that enable them to absorb and emit photons from ultraviolet (UV) to infrared region when doped into the appropriate hosts [9-15]. Recently, Lian et al synthesized the Eu^{2+} and Cu^{+} co-doped $Ca_{0.6}Sr_{0.4}S$ phosphors with a tunable dual-excitation dual-emission feature and demonstrated their effectiveness in enhancing sunlight harvesting for agricultural plants [16]. Notably, to simultaneously realize efficient blue and red emissions for photosynthesis, two different emitting activators are generally required to locate into a sole host. Unfortunately, such design usually induces the adverse energy transfers between them and subsequently results in the luminescent quenching of both activators [17-21].

Herein, europium single-doped oxyfluoride glasses with special designed glass compositions (SiO_2-Al_2O_3-NaF-YF_3) were successfully fabricated by a melt-quenching route. Interestingly, Eu^{2+} activators with blue-emitting and Eu^{3+} ones with red-emitting were evidenced to coexist in the glass synthesized under air atmosphere, which can be well explained based on optical basicity model of glass. To suppress adverse energy transfer between Eu^{2+} and Eu^{3+}, crystallization strategy was successfully applied to convert the precursor glasses into nano-glass-ceramics. As a consequence, Eu^{3+} ions were found to incorporate into the precipitated orthorhombic YF_3 nanophase, while Eu^{2+} ones remained in the glass matrix. Such spatial separation of the different active ions can effectively suppress unwanted

energy transfer between Eu^{2+} and Eu^{3+}, leading to both intense blue and red luminescence in the nano-glass-ceramics.

Experimental section

The materials were prepared with the following composition (in mol%): (44-x) SiO_2-28Al_2O_3-17NaF-11YF_3-xEuF_3 (x =0.1, 0.25, 0.5, 1.0, 2.0 and 4.0). The chemicals were mixed thoroughly and melted in a covered Pt crucible at 1450 ℃ for 30 min in the ambient atmosphere. The melt was poured into a 300 ℃ pre-heated copper mold to form the precursor glass (denoted as PG1, PG2, PG3, PG4, PG5 and PG6 for x=0.1, 0.25, 0.5, 1.0, 2.0 and 4.0 respectively). The as-quenched glass was annealed at 515 ^{0}C for 2 h and then cooled down naturally to room temperature to relinquish the inner stress. The annealing temperature is chosen to be 50 ^{0}C below the glass transition temperature (565 ^{0}C) determined by differential scanning calorimety (DSC) measurement. Afterwards, the precursor glass was then heat-treated to 670 ℃ with a heating rate of 10K/min, and hold for 2 h to form glass ceramic (denoted as GC1, GC2, GC3, GC4, GC5 and GC6 for x=0.1, 0.25, 0.5, 1.0, 2.0 and 4.0 respectively) through fluoride crystallization. Notably, the influence of the variation of glass composition on the glass crystallization has also been investigated. It was found that the NaF and YF_3 composition contents should be in the range of 15-20 mol% and 7-15 mol% respectively to realize the precipitation of YF_3 crystalline phase in glass (the total mole fraction of SiO_2 and Al_2O_3 should not be lower than 65 mol%). In addition, the substitution of NaF by LiF in glass composition had no impact on the YF_3 crystallization.

DSC experiment of the as-quenched precursor glass was recorded in air at a heating rate of 10 K/min in order to follow its thermal behavior. The actual composition of the glass was detected by X-ray photoelectron spectroscopy (XPS) using a VG Scientific ESCA Lab Mark II spectrometer equipped with two ultra-high vacuum 6 (UHV) chambers. All the binding energies were referenced to the C_{1s} peak of the surface adventitious carbon at 284.8 eV. To identify the crystallization phase and determine the mean size of crystallites, x-ray diffraction (XRD) analysis was carried out with a powder diffractometer (DMAX2500 RIGAKU) using CuK_{α} radiation (λ=0.154nm). The microstructure of GC was studied using a transmission electron microscopy (TEM, JEM-2010) equipped with an energy dispersive X-ray (EDX) spectroscopy and the selected area electron diffraction (SAED). TEM specimen was prepared by directly drying a drop of a dilute ethanol dispersion solution of glass pieces on the surface of a carbon coated copper grid. The optical transmission spectra were recorded by a spectrophotometer (Lambda900, Perkin-Elmer) with a resolution of 1 nm. The emission, excitation spectra and Eu^{3+} decay curves of PGs and GCs were recorded on an Edinburgh Instruments FS5 spectrofluoremeter equipped with both continuous (150 W) and pulsed xenon lamps. The Eu^{2+} decay curves of the PG and GC samples were detected on an Edinburgh Instruments FLS920 spectrofluoremeter equipped with a 375nm picosecond pulsed diode laser (EI-EPL-375). Quantum yield (QY), defined as the ratio of the emitted photons to the absorbed photons, is calculated based on the following equitation:

$$\eta = \frac{number\ of\ \ photons\ emitted}{number\ of\ \ photons\ absorbed} = \frac{L_{sample}}{E_{reference} - E_{sample}} \qquad (1)$$

where η represents QY, L_{sample} the emission intensity, $E_{reference}$ and E_{sample} the intensities of excitation light not absorbed by reference and sample respectively. The measurements were detected on the FS5 spectrofluoremeter equipped with an integrating sphere. All the measurements were carried out at room temperature.

Results and discussion

Table 1 Nominal and actual composition (mol%) of glass

Element	Nominal	Actual
Si	11.30	11.51
Al	15.82	16.11
Na	4.80	4.43
Y	3.11	2.99
Eu	1.13	1.09
O	46.33	47.17
F	17.51	16.70

The XPS measured actual composition of the $40SiO_2$-$28Al_2O_3$-17NaF-$11YF_3$-$4EuF_3$ glass, together with its nominal composition (in mol%), is tabulated in Table 1. Noticeably, compared with the nominal ones, the actual contents of Na, Y, Eu and F elements are more or less reduced, which is due to the thermal evaporation of the fluoride raw materials during high-temperature melting. Fortunately, the slight decrease of fluoride compositions has no obvious impact on the YF_3 crystallization.

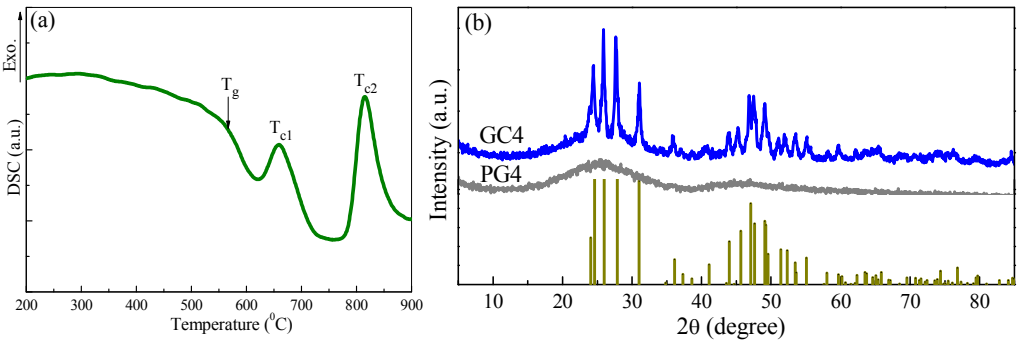

Figure 1 (a) DSC curve of the as-quenched PG4 glass recorded at a heating rate of 10K/min. (b) XRD patterns of PG4 and GC4; bars represent the diffraction pattern of the standard orthorhombic β-YF_3 (JCPDS No. 74-0911) phase.

Figure 1a shows the DSC curve of the precursor glass where T_g (565 °C), T_{c1} (670 °C) and T_{c2} (812 °C) stand for the glass transition temperature, the fluoride crystallization temperature and the bulk crystallization temperature of glass matrix respectively, as evidenced by XRD analyses. The large differences up to 105 °C between glass transition temperature and the fluoride crystallization temperature and 147 °C between the fluoride crystallization temperature and the bulk glass crystallization temperature provide the possibility to control the precipitation and growth of the fluoride crystallites among the glass matrix.

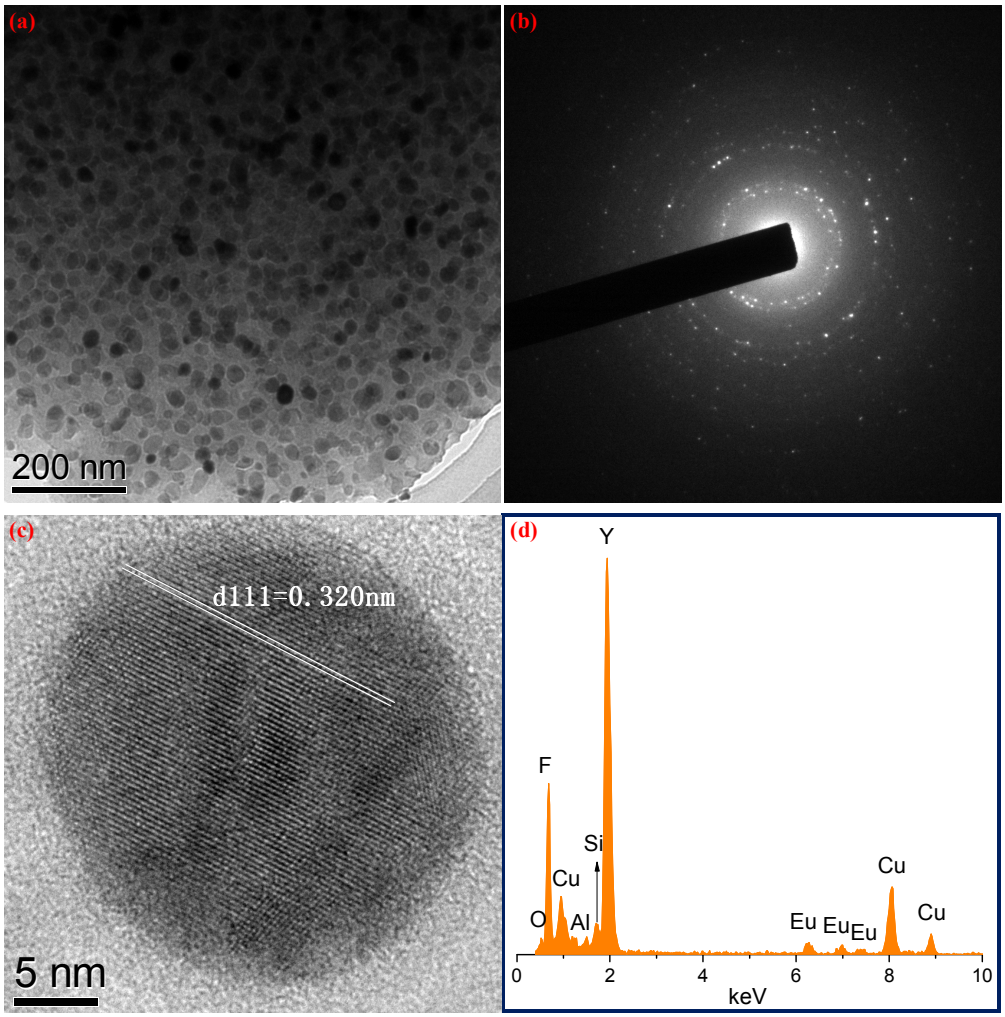

Figure 2 (a) TEM image and (b) SAED pattern of GC4; (c) HRTEM micrograph and (d) EDX spectrum of an individual NC in GC4. The presence of Cu peaks in EDX spectrum is due to copper grid used to support TEM specimen.

XRD patterns of the PG4 and GC4 samples are presented in Figure 1b. The precursor glass is amorphous without any sharp signals. After crystallization, the XRD pattern shows intense diffraction peaks assigned to the orthorhombic β-YF_3 crystals (JCPDS No. 74-0911). The mean size of the crystals was calculated to be about 20 nm by the Scherrer formula. The volume fraction of the crystalline phase estimated by the ratio of the integrated area of the peaks and the total XRD pattern is about 32 %. TEM image of the GC4 sample (Figure 2a) demonstrates that nanocrystals (NCs) sized 15-25 nm are distributed homogeneously among the glass matrix with their selected area electron diffraction rings well indexed to the orthorhombic β-YF_3 (Figure 2b). High-resolution TEM (HRTEM) image of an individual NC in GC4 presented in Figure 2c exhibits clear-cut YF_3 lattice structure. In order to detect the distribution of europium ions in the glass ceramic, the EDX spectrum (Figure 2d), taken from an individual nanocrystal, exhibits Y, F and Eu signals, the weak Al, Si, and O ones are attributed to the glass matrix surrounding the nanosized crystal. Notably, the presence of Cu peaks in the spectrum is originated from copper grid used to support TEM specimen. This result indicates that europium ions partition into the precipitated YF_3 lattice after glass crystallization.

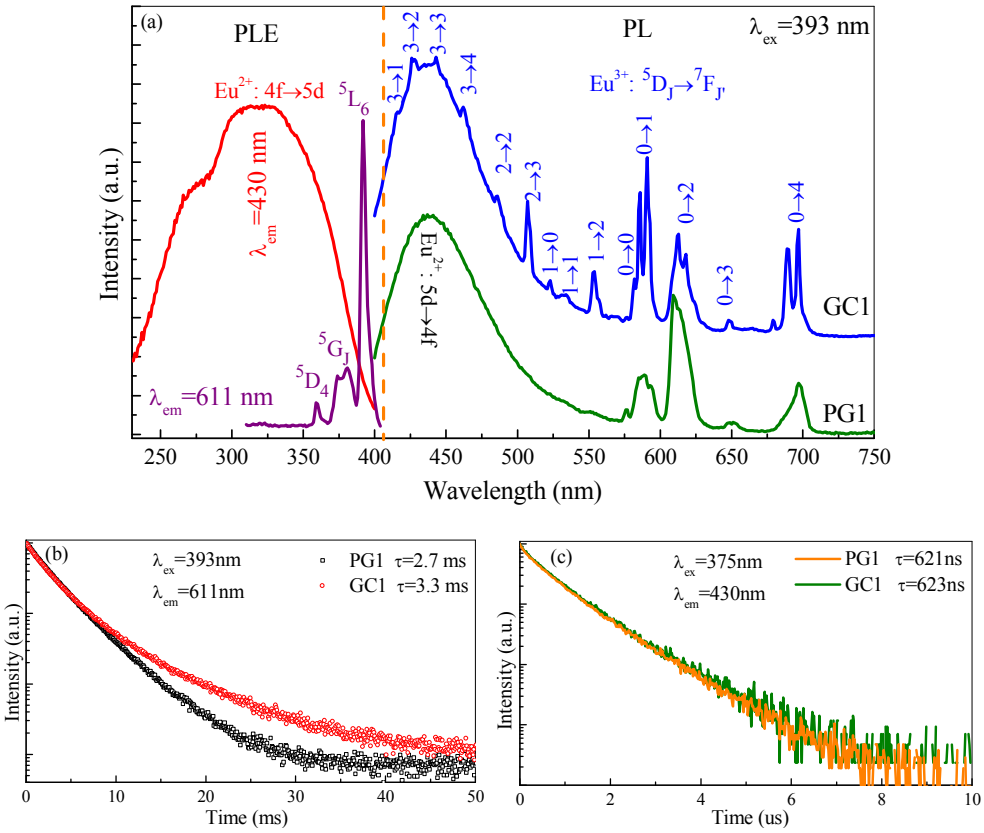

Figure 3 (a) Photoluminescence (PL) and PL excitation (PLE) spectra of PG1 and GC1 samples. Decay curves corresponding to (b) Eu^{3+}: $^5D_0$ and (c) Eu^{2+}: 5d states in PG1 and GC1 samples.

The optical transmission spectrum of the GC1 sample has been recorded, as exhibited in Figure S1 (Electronic Supplementary Information). The transmittance of the sample reaches 83% within the range of the visible light wavelength, which verifies the good transparency of the investigated nano-glass-ceramic. Room temperature excitation and emission spectra of PG1 and GC1 samples are shown in Figure 3a. The excitation spectra consist of Eu^{3+} characteristic excitation lines within $4f^6$ configuration in the UV-violet region. The strongest excitation peak at 393 nm is assigned to the Eu^{3+}: $^7F_0 \rightarrow {}^5L_6$ transition. The emission spectra for the PG1 and GC1 under 393 nm excitation exhibit the PL bands of the transitions from the excited ^5D_J level to the lower $^7F_{J'}$ ones of Eu^{3+}. The emission bands of PG1 are inhomogeneouly

broadened, while those of GC1 become remarkably structured in a way similar to the case of the Eu^{3+} doped YF_3 crystal [22]. Besides, it is noticeable that the luminescence originated from the $^5D_{1,2,3}$ levels appears in GC1. All these changes in optical performance can be taken as an indicator of the different surroundings for Eu^{3+} ions before and after crystallization, i.e., Eu^{3+} ions enter into YF_3 lattice, which is further confirmed by the longer decay time of GC1 than that of PG1, as shown in the Figure 3b.

Notably, the Eu^{3+} $^5D_{1,2,3}$ emission intensities of GC1 are far stronger than those of PG1, as revealed in Figure S2 (Electronic Supplementary Information). For Eu^{3+} ions, the higher excited states $^5D_{1,2,3}$ can be easily quenched through multi-phonon relaxation when the maximum phonon energy of the host lattice is high enough. The energy gap to the next lower level of Eu^{3+}: $^5D_1$, $^5D_2$ and $^5D_3$ is about 1600, 2500, and 2700 cm^{-1}, respectively. It was reported that the maximum phonon energy of the precursor glass is about 1100 cm^{-1} [23], while that of YF_3 where Eu^{3+} resided is around 400 cm^{-1} [24]. Therefore, two to three phonons are required to bridge the energy gaps between the two neighbor levels in the precursor glass, while four to seven phonons are needed for the glass ceramic, which results in the lower non-radiative multi-phonon relaxation probability of GC1 than that of PG1.

The spectroscopy of the $^5D_0$ level is another useful tool to investigate the location of Eu^{3+}. The intensity ratio (β) of $^5D_0 \rightarrow {}^7F_2$ and $^5D_0 \rightarrow {}^7F_1$ transitions is determined by the symmetry of the crystal sites in which Eu^{3+} ions are located. From the emission spectra, β is evaluated to be 2.07 and 0.69 for PG1 and GC1,

respectively. The intensity of the magnetic dipolar $^5D_0 \rightarrow {}^7F_1$ transition does not depend on the ligand field of Eu^{3+}, while the electric dipolar $^5D_0 \rightarrow {}^7F_2$ transition is known to be forbidden in the centrosymmetric environment [25]. Apparently, the decrease of β after crystallization is caused by the increase in symmetry of the Eu^{3+} ligand field, which further evidences the incorporation of Eu^{3+} into the YF_3 lattice by substituting Y^{3+}.

Besides the sharp emissions of Eu^{3+}, a very intense broadband blue emission centered at 430 nm is also detected in both the PG1 and GC1 samples, as shown in Figure 3a, which is believed originated from the Eu^{2+} 5d→4f transition. A similar broadband emission has been reported in the Eu^{2+} doped GCs containing CaF_2 NCs previously [26-27]. The characteristic excitation spectrum of Eu^{2+} ions in the GC1 sample is also provided in Figure 3a. The excitation band with a maximum at 330 nm corresponding to the Eu^{2+} 4f→5d transition is recorded when monitored at 430 nm emission. The luminescence decay curves for Eu^{2+} in both PG1 and GC1 (Figure 3c) exhibit a nearly single exponential decay with the lifetimes of 621 and 623 ns, respectively. The lifetime in nanosecond order is one of the characteristics of the Eu^{2+} electric-dipole allowed 5d→4f transition [28]. Fu et al. [26-27] found that the Eu^{2+} emission in the glass ceramic containing CaF_2 NCs was much stronger than that in the precursor glass, due to the partition of Eu^{2+} ions into the CaF_2 crystalline phase. However, for the presently investigated PG1 and GC1 samples, the emission intensity and lifetime of Eu^{2+} (Figure 3c) are not obviously modified after glass crystallization, revealing that Eu^{2+} ions do no enter into the YF_3 NCs but stay in the glass matrix. This

result is reasonable since the radius of Eu^{2+} (0.139 nm, CN=6) is far larger than that of Y^{3+} (0.104 nm, CN=6), and the charge compensations are necessary for the substitution of Y^{3+} by Eu^{2+} in the crystal lattice.

Normally, the formation of Eu^{2+} is not expected in glasses fabricated in the ambient condition. In order to retain Eu^{2+} ionic state while using EuF_3, i.e., Eu^{3+}, as the precursor raw material, a reducing atmosphere is generally required to promote the reduction. The existence of Eu^{2+} ions in the present glass system obtained by air atmospheric condition can be well explained based on optical basicity model proposed by Duffy et al [29-30]. It has been predicted that the glass with lower optical basicity below a certain critical value will favor the conversion of a higher oxidation state to a lower one for a multivalent cation. As for europium, the occurrence of $Eu^{3+} \rightarrow Eu^{2+}$ conversion will be realized in any glass system synthesized in air atmosphere only when its optical basicity is below a critical value of 0.585. Using Duffy's empirical formula [20-30], the optical basicity of the present glass is calculated to be 0.511 based on the amount of oxygen or fluorine in each oxide or fluoride and their corresponding basicity values [29-31]. Thus, formation of Eu^{2+} has been promoted in the present system as the optical basicity value is far lower than the reported critical optical basicity (0.585). In fact, compared to pure oxide glass, the presence of F^- ions along with O^{2-} Ions in the oxyfluoride glass network causes a reduction of optical basicity, which is beneficial to the conversion of Eu^{3+} to Eu^{2+} under normal air atmosphere [31-33]. To prove this point, the Na_2O composition was used to replace the NaF one in the glass. As a consequence, no Eu^{2+} emission but

only pure Eu^{3+} luminescence is detected since the optical basicity of this glass with low fluorine content is higher than the required critical value.

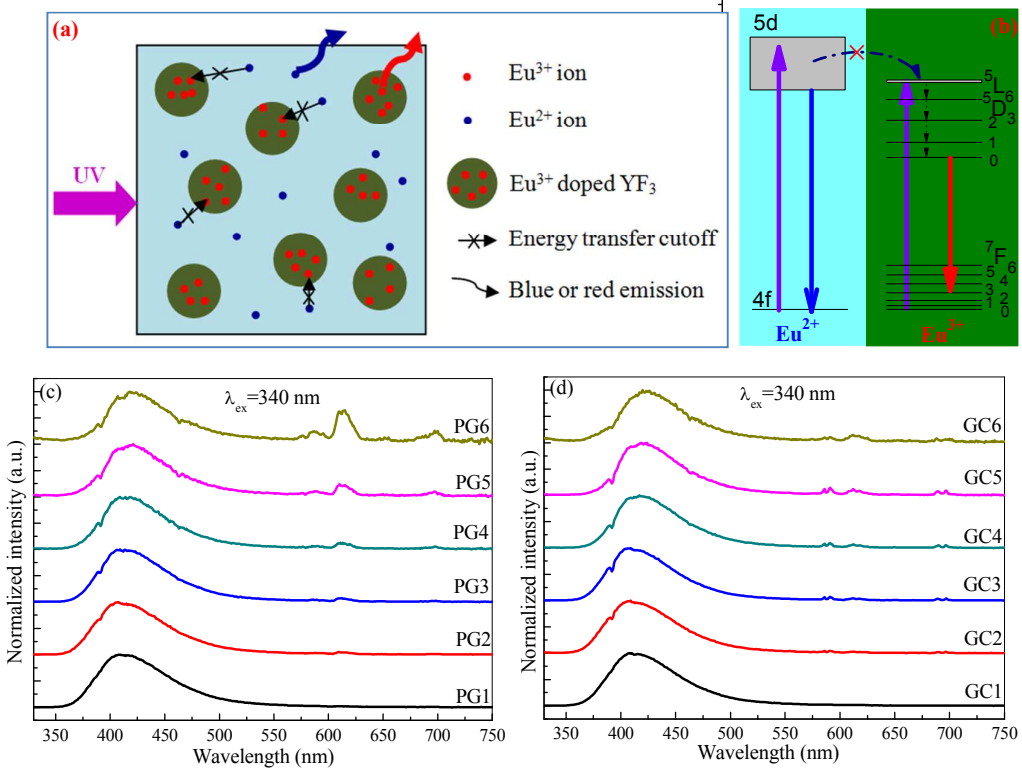

Figure 4 (a) A sketch showing the distribution and luminescent behaviors of Eu^{2+} and Eu^{3+} ions in GC; (b) Schematic energy level diagrams of Eu^{2+} and Eu^{3+} ions showing the suppression of energy transfer when Eu^{3+} ions are partitioned into YF_3 nanophase; Emission spectra of (c) PGs and (d) GCs doped with various contents of europium under 340 nm light excitation.

After such glass structural design, Eu^{3+} ions incorporated into the precipitated YF_3 nanophase, while Eu^{2+} ones remained in the glass matrix, as schematically shown in Figure 4a. As expected, this spatial isolation strategy for the different active ions should effectively lessen adverse energy transfer between Eu^{2+} and Eu^{3+} (Figure 4b), leading to both intense blue and red emissions originated from Eu^{2+} and Eu^{3+} respectively. To prove this point, PL spectra of both PGs and GCs doped with various contents of europium were recorded under 340 nm light excitation corresponding to Eu^{2+}: 4f→5d absorption transition, as shown in Figure 4c-4d. In order to clearly

present the relative intensity variation between Eu^{2+} and Eu^{3+}, all the spectra are normalized to Eu^{2+} emission band. With increase of europium doping content, the Eu^{3+} emission intensity relative to Eu^{2+} one gradually enhances for PGs, while the Eu^{3+} emission is always very weak for GCs. Since Eu^{3+} ions cannot be excited under 340 nm light excitation, these results evidence the existence of energy transfer from Eu^{2+} to Eu^{3+} in the PG samples and the efficient suppression of energy transfer between them in the GC samples. The decay profiles for both PGs and GCs doped with various contents of europium by recording Eu^{2+} 430 nm emission under 340 nm light excitation are provided in Figure 5, and the corresponding lifetime values are calculated, as tabulated in Table 2. With increase of europium doping content, the conversion fraction of Eu^{3+} to Eu^{2+} will increase, which results in the gradual decrease of Eu^{2+} lifetime in both PG and GC due to concentration quenching effect. However, compared to the case of PG, the corresponding lifetime of GC is always longer, as evidenced in Table 2, confirming the successful suppression of energy transfer between Eu^{2+} and Eu^{3+} via “dopant isolation” strategy.

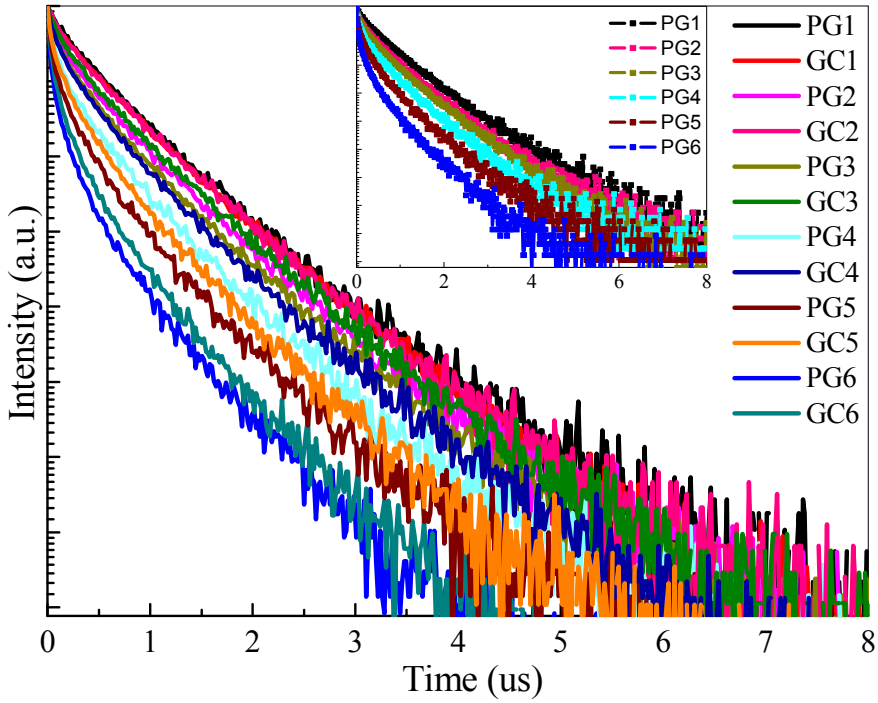

Figure 5 Decay curves of PGs and GCs corresponding to Eu^{2+}: 5d→4f transition (λ_{em}=430 nm) under 340 nm light excitation.

Table 2 Dependence of Eu^{2+} lifetime on europium doping content

Europium content (mol%)	Eu^{2+} lifetime in PG (ns)	Eu^{2+} lifetime in GC (ns)
0.1	621	623
0.25	473	611
0.5	419	516
1	305	397
2	215	278
4	127	178

Ultimately, the simultaneous tuning into blue and red from UV excitation in PGs and GCs is demonstrated under different wavelength light excitation, as exhibited in Figure 6. Two typical excitation wavelength lights, i.e., 365 and 393 nm, were adopted to excite the samples. As evidenced in the PLE spectra of Figure 3a, both input lights can simultaneously excite Eu^{2+} and Eu^{3+} ions in the samples. The difference is that the 365 nm light predominantly excites Eu^{2+} while 393 nm light mainly excites Eu^{3+}. Under 365/393 nm light excitation, the intensity ratio of

red-emitting (Eu^{3+}) to blue-emitting (Eu^{2+}) in both PGs and GCs enhances with increase of europium content. Especially, under 365 nm light excitation, the suppression of energy transfer from Eu^{2+} to Eu^{3+} in the GCs results in the existence of more Eu^{2+} blue-emitting component than that of the PGs. The emission spectra of the PGs and GCs doped with various contents of europium can be easily converted to the Commission International de I'Eclairage (CIE) 1931 chromaticity diagram, as plotted in Figure 7. With increase of europium content, the luminescent color changes from blue to red. Evidently, the moving of color coordination from blue to red in the GCs is always slower than that in the PGs due to the efficient suppression of energy transfer from Eu^{2+} to Eu^{3+}. As a consequence, GCs predominantly show blue emission under 365 nm light excitation, while they mainly exhibit red radiation when the excitation light wavelength is modified into 393 nm.

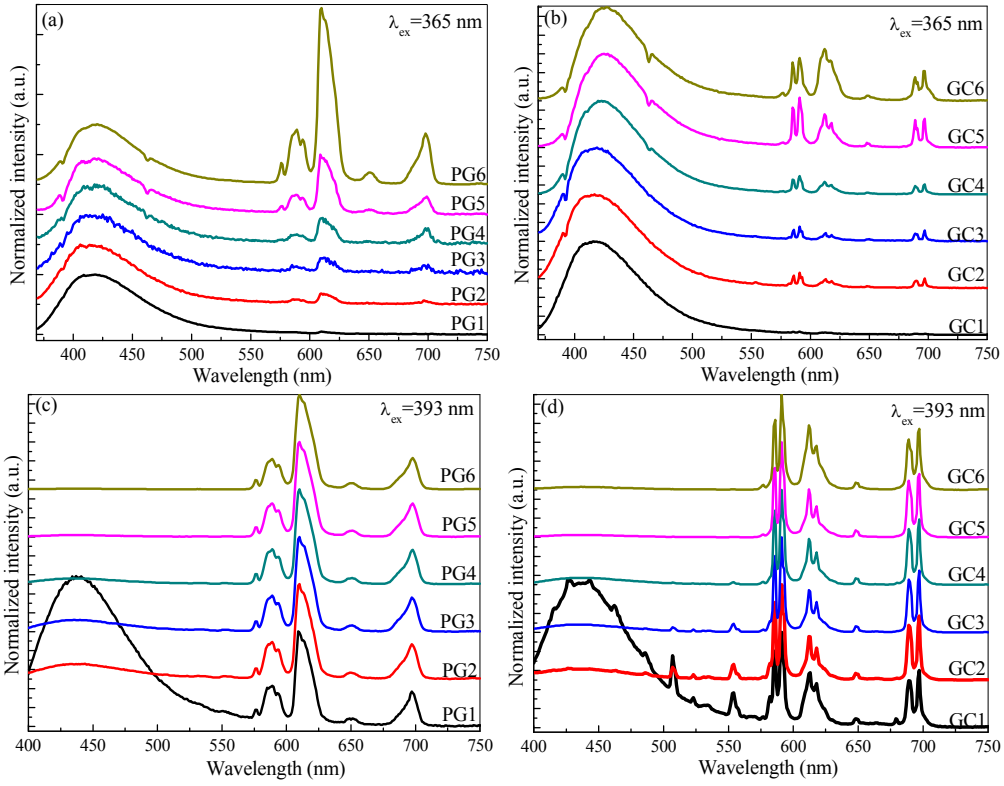

Figure 6 Emission spectra of the (a, c) PGs and the corresponding GCs (b, d) under 365 nm and 393 nm light excitation respectively.

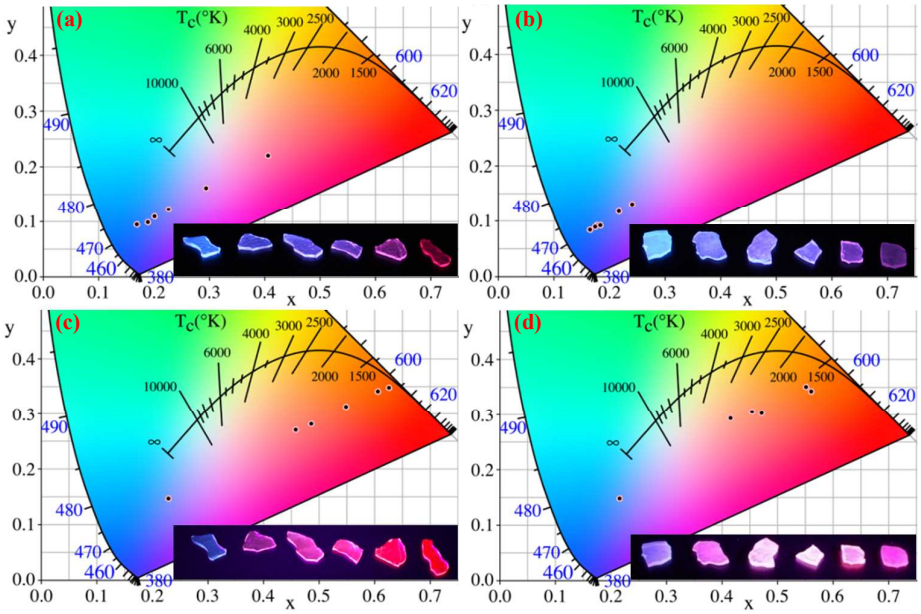

Figure 7 CIE coordinate diagram showing chromaticity points of europium luminescence: (a) PGs under 365 nm light excitation, (b) GCs under 365 nm light excitation, (c) PGs under 393 nm light excitation, (d) GCs under 393 nm light. For each diagram, data points from left to right are assigned to samples with europium contents of 0.1, 0.25, 0.5, 1, 2 and 4 mol.%, respectively. Insets are UC luminescent photographs of the corresponding samples.

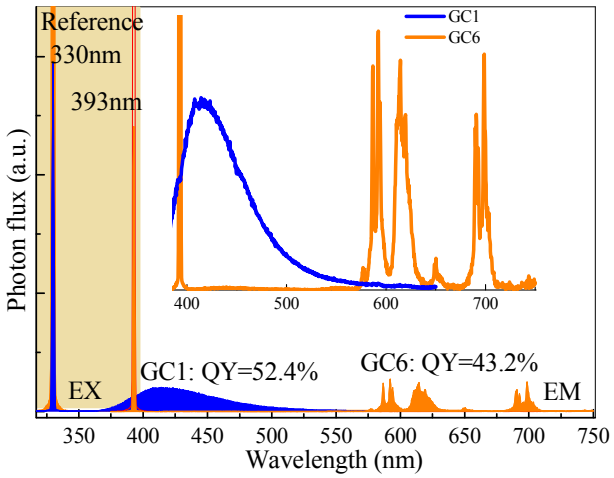

Figure 8 Quantitative excitation and emission spectra of GC1, GC6 and reference samples recorded by a spectrofluoremeter equipped with an integrating sphere for QY measurement. The inset shows the magnified emission spectra in the wavelength range of 400-750 nm.

Using an integrated sphere, the quantitative excitation and emission spectra in the wavelength region (320-750nm) for the PG1/GC1 (under 330 nm light excitation) and PG6/GC6 (under 393 nm light excitation) were recorded, as exhibited in Figure 8.

Accordingly, the PL QYs were calculated as 47.3%/52.4% and 23.3%/43.2%, respectively. The higher QY (52.4%) of Eu^{2+} emission in GC1 than that (47.3%) in PG1 is due to the suppression of energy transfer from Eu^{2+} to Eu^{3+} in GC1; whereas the nearly two-fold enhanced QY of Eu^{3+} emission in GC6 (43.2%) compared to that in PG6 (23.3%) is ascribed to the incorporation of Eu^{3+} into the low-phonon-energy YF_3 lattice, which results in a low non-radiative multi-phonon relaxation probability for Eu^{3+}. As depicted in Figure 9, the standard terrestrial (AM1.5) solar irradiation spectrum covers ultra-broad wavelength region from ultraviolet to infrared. However, the chlorophylls mainly absorb reddish orange (600-700 nm) and bluish violet (380-480 nm) lights in the course of the photosynthesis, i.e., the lights used by green plants for photosynthesis are only a very small part in the whole solar spectra. The investigated GCs, which can convert the UV photons into blue/red ones, may find potential application in photosynthesis of green plants by improving the utilization of solar in the future.

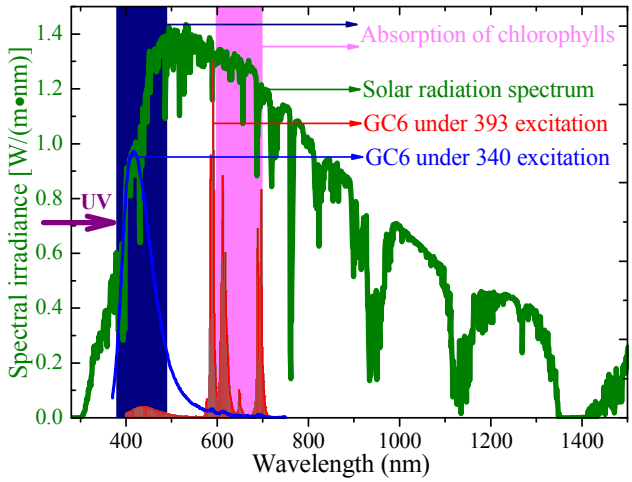

Figure 9 Schematic illustration showing the conversion of UV photons into blue and red ones by using GC6 sample, which are located in the absorption regions of chlorophylls.

Conclusions

In summary, europium single-doped oxyfluoride glasses were successfully synthesized by the melt-quenching route. The in situ formation of divalent europium (Eu^{2+}) along with Eu^{3+} during high-temperature synthesis of these glasses in air atmosphere was evidenced and explained based on optical basicity model. After crystallization, orthorhombic β-YF_3 nanocrystals embedded glass ceramics were achieved where Eu^{3+} ions were confirmed to incorporate into the crystalline lattice while Eu^{2+} ones remained in glass matrix. As a consequence, the energy transfer from Eu^{2+} to Eu^{3+} was greatly reduced due to the spatial separation of these two different active ions, which is beneficial to the realization of both intense blue emission ascribing to Eu^{2+}: 5d→4f transition and red luminescence corresponding to Eu^{3+}: $^5D_0 \rightarrow {}^7F_J$ transitions under ultraviolet light excitation. We believed that the investigated glass ceramics, which can convert the ultraviolet photons into blue/red ones, have potential application in photosynthesis of green plants after further optimizing glass-ceramic structure and optical performance.

Acknowledgements

This work was supported by the National Natural Science Foundation of China (21271170, 51372172, 61372025 and 51402077).

References

[1] R. E. Blankenship, D. M. Tiede, J. Barber, G. W. Brudvig, G. Fleming, M. Ghirardi, M. R. Gunner, W. Junge, D. M. Kramer, A. Melis, et al, *Science*, 2011, **332**, 805.

[2] L. Wondraczek, M. Batentschuk, M. A. Schmidt, R. Borchardt, S. Scheiner, B. Seemann, P. Schweizer and C. J. Brabec, *Nat. Commun.*, 2013, **4**, 2047.

[3] C. Ming, F. Song, X. Ren and L. An, *Appl. Phys. Lett.*, 2013, **103**, 041906.

[4] C. Ming, F. Song, L. An and X. Ren, *Appl. Phys. Lett.*, 2013, **102**, 141903.

[5] D. Q. Chen, Y. S. Wang and M. C. Hong, *Nano Energy*, 2012, **1**, 73.

[6] N. Bloembergen, *Phys. Rev. Lett.*, 1959, **2**, 84.

[7] C. Ronda, *J. Alloys Compd.*, 1995, **225**, 543.

[8] X. Y. Huang, S. Y. Han, W. Huang and X. G. Liu, *Chem. Soc. Rev.*, 2013, **42**, 173.

[9] F. Wang and X. G. Liu, *Chem. Soc. Rev.*, 2009, **38**, 976.

[10] E. H. Song, J. L. Wang, D. C. Yu, S. Ye and Q. Y. Zhang, *J. Mater. Chem. C*, 2014, **2**, 8811.

[11] Y. J. Li, S. Ye and Q. Y. Zhang, *J. Mater. Chem. C*, 2014, **2**, 4636.

[12] D. Q. Chen, Y. Chen, H. W. Lu and Z. G. Ji, *Inorg. Chem.*, 2014, **53**, 8638.

[13] Y. Li, Y. Y. Li, K. Sharafudeen, G. P. Dong, S. F. Zhou, Z. J. Ma, M. Y. Peng and J. R. Qiu, *J. Mater. Chem. C*, 2014, **2**, 2019.

[14] G. Y. Chen, H. L. Qiu, P. N. Prasad and X. Y. Chen, *Chem. Rev.*, 2014, **114**, 5156.

[15] S. L. Gai, C. X. Li, P. P. Yang and J. Lin, *Chem. Rev.*, 2014, **114**, 2343.

[16] S. Lian, C. Rong, D. Yin and S. Liu, *J. Phys. Chem. C*, 2009, **113**, 6298.

[17] S. F. Zhou, N. Jiang, K. Miura, S. Tanabe, M. Shimizu, M. Sakakura, Y. Shimotsuma, M. Nishi, J. R. Qiu and K. Hirao, *J. Am. Chem. Soc.*, 2010, **132**, 17945.

[18] D. Q. Chen, L. Lei, A. P. Yang, Z. X. Wang and Y. S. Wang, *Chem. Commun.*, 2012, **48**, 5898.

[19] R. Zhang, H. Lin, D. Q. Chen, Y. L. Yu and Y. S. Wang, *J. Alloys Compd.*, 2013, **552**, 398.

[20] H. Lin, R. Zhang, D. Q. Chen, Y. L. Yu, A. P. Yang and Y. S. Wang, *J. Mater. Chem. C*, 2013, **1**, 1804.

[21] H. L. Wen, H. Zhu, X. Chen, T. F. Hung, B. L. Wang, G. Y. Zhu, S. F. Yu and F. Wang, *Angew. Chem. Int. Edit.*, 2013, **52**, 13419.

[22] B. Q. Shao, Q. Zhao, N. Guo, Y. C. Jia, W. Z. Lv, M. M. Jiao, W. Lu and H. P. You, *Cryst. Growth Des.*, 2013, **13**, 3582.

[23] D. Zhao, X. Qiao, X. Fan and M. Wang, *Physica B*, 2007, **395**, 10.

[24] M. M. Lage, A. Righi, F. M. Matinaga, J. Y. Gesland and R. L. Moreira, *J Phys: Condens Matter.*, 2004, **16**, 3207.

[25] D. Q. Chen, Y. L. Yu, P. Huang, H. Lin, Z. F. Shan and Y. S. Wang, *Acta Mater.*, 2010, **58**, 3035.

[26] J. Fu, J. M. Parker, P. S. Flower and R. M. Brown, *Mater. Res. Bull.*, 2002, **37**, 1843.

[27] M. Itoh, T. Sakurai, T. Yamakami and J. Fu, *J. Lumin.*, 2005, **112**, 161.

[28] D. Q. Chen, Y. S. Wang, Y. L. Yu, P. Huang and F. Y. Weng, *J. Phys. Chem. C*, 2008, **112**, 18943.

[29] J. A. Duffy, *Phys. Chem. Glasses*, 2005, **46**, 1.

[30] J. A. Duffy, *Phys. Chem. Glasses*, 2011, **52**, 107.

[31] K. Biswas, S. Balaji, D. Ghosh, A. D. Sontakke and K. Annapurna, *J. Alloys Compd.*, 2014, **608**, 266.

[32] K. Biswas, S. Balajji, P. Karmakar and K. Annapuran, *Opt. Mater.*, 2015, **39**, 153.

[33] K. Biswas, A. D. Sontakke, R. Sen and K. Annapurna, *J. Fluoresc.*, 2012, **22**, 745.

Graphic Abstract

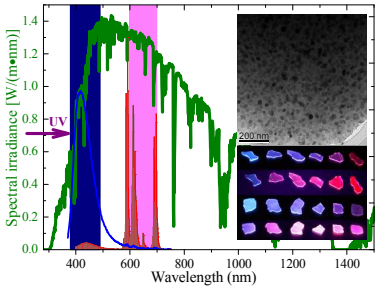

Nano-glass-ceramics, which can convert ultraviolet photons into blue/red ones, were explored for potential application in photosynthesis of plants.